18TH WORLD CONFERENCE ON EARTHQUAKE ENGINEERING
WCEE2024
MILAN

MILAN, ITALY
30TH JUNE - 5TH JULY 2024
www.wcee2024.it

INVESTIGATING NEAR-FAULT EFFECTS ON SOIL LIQUEFACTION USING STOCHASTICALLY SIMULATED GROUND MOTIONS

A.J. Makdisi[1], M. Dabaghi[2], L. Brito[3], S. Rezaeian[1], K.L. Haynie[1], & H.B. Mason[1,4]

[1] U.S. Geological Survey, Golden, Colorado, USA, amakdisi@usgs.gov

[2] American University of Beirut, Beirut, Lebanon

[3] University of Colorado, Boulder, Colorado, USA

[4] Oregon State University, Corvallis, Oregon, USA

Abstract: *The scarcity of historically recorded near-fault ground motions poses a challenge to systematically understanding the influence of near-fault effects on various types of seismic demands for engineering purposes. In particular, the current state of knowledge of the influence of ground-shaking intensity on soil liquefaction and its consequences does not specifically account for the effects of near-fault ground motion characteristics. In this study, the influence of near-fault ground motions on liquefaction triggering and lateral spreading are investigated using non-linear modeling of a hypothetical liquefiable soil column in the finite-element computational platform OpenSees subjected to simulated ground motion time series that represent strong earthquake shaking in the near field. The simulated ground motion time series and resulting datasets are based on a parametric stochastic model and are developed for a range of source and path parameters to represent a realistic variability of ground motion characteristics. Dependencies between ground motion intensity measures (IMs) and liquefaction demand parameters are investigated for near-fault pulse and non-pulse-like ground motion sets. Evolutionary IMs, such as cumulative absolute velocity (CAV) and the time-varying magnitude-adjusted peak ground acceleration (PGA_M), are considered in developing liquefaction triggering probability density functions. Post-liquefaction triggering responses such as lateral spreading displacements are examined in relation to PGA_M and CAV. The ground motion simulations are validated by comparing their liquefaction-capacity PGA_M fragilities and post-triggering CAV vulnerability relationships to historical records from the 1994 Northridge earthquake in California, USA. Finally, a path forward for future studies that includes finding systematic differences in the IM-liquefaction demand relationships between near-fault and far-field stochastic ground motion sets is outlined.*

1. Introduction

Ground failure initiated by earthquake-induced soil liquefaction (herein “liquefaction”) can cause substantial damage to critical infrastructure. Although the mechanics of liquefaction at smaller scales have been extensively examined by laboratory testing, the system-level response of liquefaction-susceptible sites subjected to strong earthquake motions is less well-understood. System-level liquefaction response is complex and difficult to rigorously observe and quantify from field case histories, and these challenges make liquefaction hazards difficult to forecast for future earthquakes. Characterization of liquefaction hazards is further complicated in regions within about 30 km of the earthquake rupture (i.e., the *near-fault* region). Although it is clear that near-fault sites experience greater ground-shaking intensities, and common liquefaction hazard evaluation procedures account for the effects of ground motion intensities on the potential for liquefaction triggering and its consequences, the effects of near-fault directivity (i.e., the occurrence of large velocity pulses) and directionality on liquefaction hazards are not well understood.

This limited understanding of near-field effects is not exclusive to liquefaction-related phenomena – there is a relative scarcity of historical recordings of near-fault motions, particularly pulse-like motions, from which to draw definitive conclusions about how pulses affect engineering responses, and whether they do so in ways

that are not adequately captured using traditional ground motion intensity measures (IMs). As a result, it is unclear in many earthquake engineering applications whether the probability of pulse-like behavior and the specific characteristics of the pulse (i.e., amplitude or period) can and should be systematically incorporated into fragility or vulnerability assessments.

Recently, the expansion of computational capacity and advances in using physics-based models and stochastic processes to numerically simulate earthquake ground motions, including near-fault characteristics such as forward directivity pulses, has allowed for a better understanding of the impacts of ground motion characteristics from events where historical data are limited (e.g., large-magnitude crustal earthquakes at close distances likely to produce velocity pulses). For instance, Kenawy et al. (2021) used near-fault simulations to assess the effects of directivity pulses on structural response and collapse risk of reinforced concrete buildings. Many of the same challenges in systematically assessing the effects of near-fault ground motion characteristics on engineering response, namely the relative lack of field observations over a wide range of earthquake and site conditions, exist in the characterization of liquefaction-related phenomena. A common method for addressing knowledge gaps in liquefaction hazard assessment is to leverage numerical models of liquefiable systems that are capable of simulating the complex, dynamic mechanics that contribute to liquefaction and its consequences. Such analyses can therefore be used to systematically assess the sensitivity of liquefaction-related phenomena to various ground motion and site conditions.

In this study, multiple simulation-based methodologies were used to examine the convergence of two phenomena that are poorly constrained from field data: near-fault ground motion effects and system response of liquefiable sites. A stochastic site-based simulation procedure was used to produce 1,000 near-fault records representing an event similar to the 1994 Northridge earthquake in California, USA, and the finite-element non-linear effective-stress analysis platform OpenSees (McKenna et al., 2010) was used to propagate those motions through a liquefiable soil column to simulate excess pore pressure generation, the onset of liquefaction triggering, and the accumulation of post-triggering permanent displacements. The analysis results were used to explore several different relationships between ground motion IMs and liquefaction demands, including hypothetical fragilities that characterize the capacity of the soil column to resist liquefaction, and vulnerability functions that relate permanent deformations to the post-triggering ground motion IMs. The liquefaction demand relationships were computed for both pulse-like and non-pulse-like ground motions, and the suitability of certain ground motion IMs for capturing pulse effects was assessed by comparing the similarity between the pulse- and non-pulse-like liquefaction demand relationships. This paper further explores potential methodologies for ground motion simulation validation (GMSV) within the context of downstream engineering uses by developing and comparing the liquefaction demand relationships using simulated motions and historical records. Potential implications of the results and future areas of refinement are discussed.

2. Simulation of near-fault ground motion time series

For this study, synthetic near-fault ground motions were generated using the Dabaghi & Der Kiureghian (2018) stochastic simulation procedure. This procedure, which builds on the site-based stochastic simulation framework of Rezaeian & Der Kiureghian (2008), generates orthogonal time series of synthetic near-fault ground motions for a set of earthquake rupture, path, and site characteristics. The procedure can simulate the observed characteristics of near-fault motions by accounting for the effects of rupture directivity, which include the likelihood and characteristics of pulse-like behavior; temporal and spectral non-stationarity of the time-series, which include ground motion characteristics such as amplitude, frequency content, and duration; and natural variability in ground motions. Use of this procedure requires specification of:

- Fault and rupture characteristics such as the style of faulting F, earthquake moment magnitude M_w, and the depth from the ground surface to the top of the rupture plane Z_{TOR};
- Path and directivity characteristics such as the closest distance from the site to the rupture plane R_{Rup} (herein the near-fault region is defined by R_{Rup} less than ~30 km), the length s (for strike-slip mechanisms) or width d (for dip-slip mechanisms) of the rupture portion that propagates from the hypocenter to the site, and the angle between the fault rupture plane and the direction between the epicenter and the site (θ for strike-slip, Φ for dip-slip);
- Site characteristics, such as the shear-wave velocity in the upper 30 m of the site (V_{S30}).

2.1. Stochastic simulations of 1994 Northridge event

Near-fault effects on liquefaction triggering and consequences were evaluated using a set of synthetic ground motions representing the magnitude-6.9 (M_w6.9) 1994 Northridge mainshock earthquake (designated as

"Northridge-01" in subsequent figures). The rupture parameters were obtained from the NGA-West2 database (Bozorgnia et al., 2014) and held fixed as inputs to the stochastic simulation model (reverse faulting, magnitude M_w = 6.69, Z_{TOR} = 5 km). Meanwhile, R_{Rup} and the directivity parameters d and Φ were computed by varying the horizontal distance from the surface projection of the top of the rupture to the site, R_x, from -30 km to 40 km in increments of 10 km, and computing the resulting path and directivity parameters from the geometric properties of the rupture as shown in Figure 1 (positive R_x values represent locations on the hanging wall, while negative values represent locations on the footwall). The site V_{S30} was held constant at 600 m/s to not include soft site amplification effects.

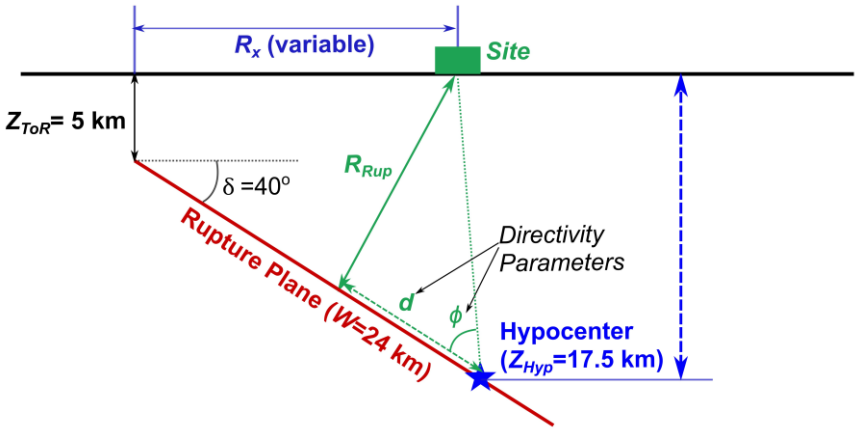

Figure 1. Schematic diagram (profile view) of 1994 Northridge rupture characteristics (reverse faulting, M_w = *6.69,* Z_{TOR} = *5 km) and associated directivity parameters.*

One hundred synthetic ground motion time series were generated for each of the 10 sites based on the varying R_x and corresponding path and rupture directivity parameters, resulting in an overall suite of 1,000 ground motion time series. For comparison with historical records, 36 records from the 1994 Northridge event were selected from the NGA-West2 database, from sites on the hanging wall or footwall. The path, site, and directivity parameters of the simulated and historical suites are summarized in Table 1. Although the ranges of path and directivity parameters are similar between the simulations and historical records, the historical records feature a much broader range of site V_{S30} values. Of the 1,000 simulations, 229 (23%) were pulse-like, while 22 out of the 36 (61%) historical records were pulse-like (per the classification criteria of Baker [2007]).

Table 1: Ranges of path, site, and directivity parameters of stochastically simulated motions representing the 1994 M_w*6.9 Northridge earthquake, with corresponding near-fault historical records from the same event.*

Source/Site Parameter	Range of simulated motions	Range from historical records
Horizontal distance from top of rupture, R_x (km)	-30 to 40 km	-37.7 to 45.15 km
Closest distance to rupture, R_{Rup} (km)	5 to 30.4 km	5.2 to 38.0 km
Directivity parameter, d (km)	0.30 to 19.4 km	4.3 to 19.4 km
Directivity parameter, ϕ (degrees)	8 to 89º	0.8 to 89º
Shear-wave velocity in upper 30 m of site, V_{S30} (m/s)	600 m/s	191 to 2,016 m/s

2.2. Validation of near-fault simulations for 1994 Northridge earthquake: Comparing IMs to GMMs and historical records

The median response spectra of the simulated motions are compared to their predicted values from empirical ground motion models (GMMs). Figure 2 shows an example of two of the 10 sites, both located 10 km away from the surface projection of the top of the rupture (R_x), but with one on the hanging wall and one of the footwall. The median GMM response spectra and their standard deviations are computed from the log-average of four NGA-West2 GMMs that are also used in the USGS National Seismic Hazard Model (Rezaeian et al., 2015), which provide predictions of the 50th percentile, orientation-independent (RotD50) spectral acceleration (Boore et al., 2006). To facilitate the most consistent comparison, the median RotD50 spectra of the 100 near-fault simulated motions are presented in Figure 2 as well. Although the Dabaghi & Der Kiureghian (2018) procedure does not explicitly use GMM-predicted response spectra to model the synthetic time series, the resulting spectra agree reasonably well with empirical GMMs. The response spectra of the pulse-like motions appear to be systematically higher than both the non-pulse-like motions and the GMM-based spectra at intermediate to long periods (as expected), mainly because the stochastic simulation procedure explicitly models directivity pulse effects (whereas traditional GMMs do not). This is most apparent at periods longer than 0.5 seconds, where velocity pulses generally occur.

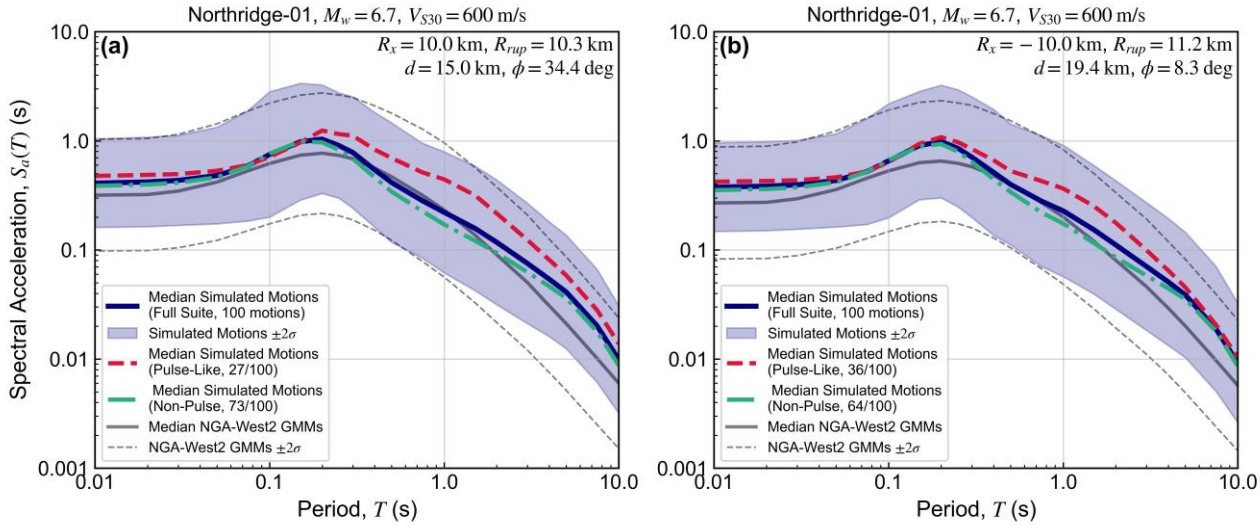

Figure 2: Response spectra of ground motion records stochastically simulated using rupture and directivity parameters consistent with the 1994 Northridge-01 earthquake at two near fault sites on the (a) hanging wall and (b) footwall. Response spectra are compared with predicted spectra using the NGA-West2 ground motion models. Solid lines represent median spectra, while shaded regions and dashed lines represent two-standard deviation ranges.

For the evaluation of liquefaction hazards, it is often advantageous to consider ground motion IMs that incorporate the combined effects of amplitude, frequency content, and duration on liquefaction response (e.g., Kramer & Mitchell, 2006). Such metrics are often referred to as *evolutionary IMs*; multiple studies have shown that these types of IMs can minimize uncertainty and bias in the estimation of liquefaction-related demand parameters, as well as account for the effects of the timing of liquefaction triggering on various liquefaction consequences (e.g., Kramer et al. 2016; Makdisi, 2016). The two evolutionary IMs considered in this study are (1) the time-varying, magnitude-adjusted peak ground acceleration PGA_M (via Kramer et al. 2016):

$$PGA_M(t) = \frac{PGA(t)}{MSF(t)} \tag{1}$$

where *PGA(t)* is the peak acceleration of the time history up until timestep *t*, and *MSF(t)* is a magnitude scaling factor that accounts for the number of equivalent cycles that have occurred at time *t*; and (2) cumulative absolute velocity *CAV*:

$$CAV = \int |a(t)|dt \quad (2)$$

Figure 3 shows the attenuation of PGA_M and *CAV* with distance for the considered suites of 1,000 simulated motions and 36 historical records used as input to the non-linear effective stress analyses (ESAs) in this study. The range of velocity pulse period T_p for the pulse-like motions is also shown in color-scale, given its importance as a characteristic of directivity pulses. For the evaluation of the IM-liquefaction demand relationships in this study, IMs were computed from the single time-series component used as input to the OpenSees ESAs. The orientation of the maximum pulse for pulse-like records was selected as the input component, while for non-pulse-like motions the orientation of maximum Arias intensity was selected (defined as the "major principal component" by Dabaghi & Der Kiureghian [2018]). The data in Figure 3 indicate consistent ranges of PGA_M and *CAV* values between the simulated motions and historical records, which enables consistent comparison of the resulting liquefaction-demand relationships.

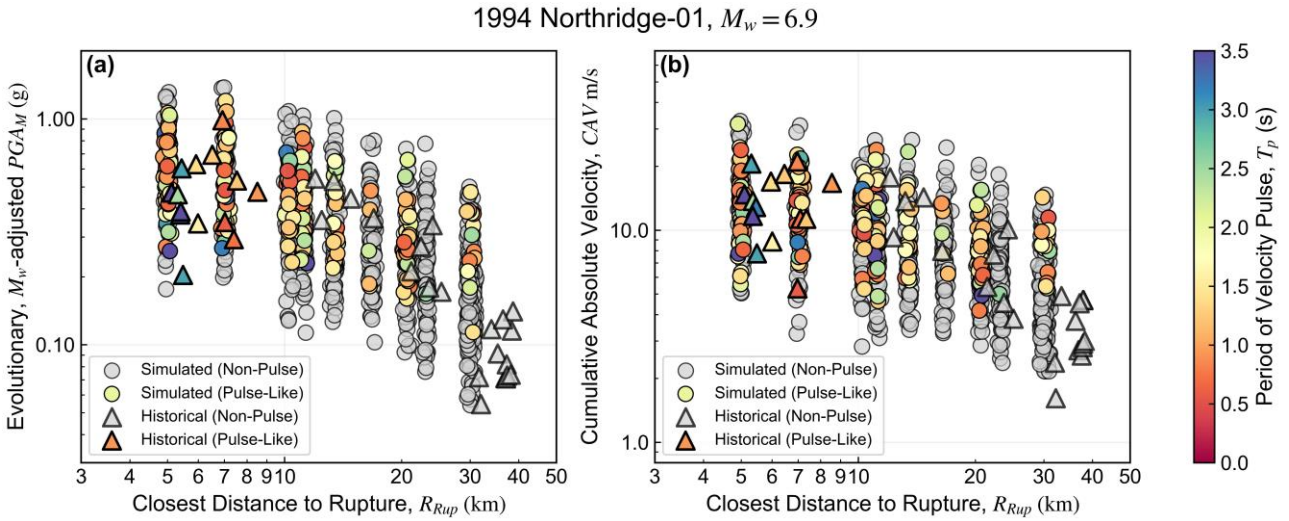

Figure 3: Attenuation of evolutionary intensity measures PGA_M *and* CAV *with closest rupture distance* R_{Rup} *for simulated and historical 1994 Northridge near-fault ground motions. Period of velocity pulse is color-mapped for pulse-like records.* R_{Rup} *values are artificially offset from their actual values for visual clarity.*

Table 2 summarizes the overall IM ranges of all simulated motions and selected historical records that were used as inputs to the liquefaction ESAs in this study. Although the pulse-like motions clearly exhibit larger values of PGA_M and *CAV* relative to the non-pulse-like motions, overlap in the IM ranges appears to be sufficient to facilitate valid comparison of the IM-liquefaction demand relationships between the two types of near-fault motions. The historical 1994 Northridge records generally exhibit higher IMs in pulse-like motions compared to the simulated motions, and much lower IMs in non-pulse-like motions. This is likely due to the manner in which the historical records are clustered in Figure 3, with a higher concentration of pulse motions within about 7 km of the rupture plane, and conversely, a higher concentration of non-pulse-like motions out at distances greater than 25 km. Nevertheless, the overall IM ranges of the historical and simulated suites appear to be similar enough to consider the simulated motions valid for estimating liquefaction-related demands in this study. Furthermore, the ranges of T_p for the simulated and historical pulse-like motions are essentially identical, indicating that the stochastic simulation procedure is capable of modelling pulse characteristics for near-fault sites in large earthquakes.

Table 2: Summary of median and 5th-95th percentile ground motion IMs of simulated and historical 1994 Northridge near-fault ground motions, used as input to non-linear effective stress models in OpenSees.

Intensity measure	Simulated Motions (1,000 records)		Historical Records (36 records)	
	Pulse-Like (229 records)	**Non-Pulse (771 records)**	**Pulse-Like (14 records)**	**Non-Pulse (22 records)**
Evolutionary, M_w-adjusted PGA_M (g)	0.47 g (0.23 – 1.01 g)	0.29 g (0.1 – 0.85 g)	0.6 g (0.4 – 1.07 g)	0.15 g (0.06 – 0.48 g)
Cumulative absolute velocity, *CAV* (m/s)	10.6 m/s (5.6 – 20.5 m/s)	7.4 m/s (3.2 – 18.7 m/s)	13.3 m/s (6.9 – 20.7 m/s)	4.6 m/s (2.4 – 14.3 m/s)
Period of velocity pulse, T_p (s)	1.5 s (0.69 – 3.2 s)	-	1.5 s (0.68 – 3.5 s)	-

3. Liquefaction response to simulated ground motions

3.1. Non-linear, effective stress, finite-element analysis of liquefiable systems

The effects of near-fault ground motion characteristics on liquefaction response were evaluated through a set of non-linear, effective stress, finite-element analyses using the open-source software platform OpenSees (McKenna et al., 2010). The general schematic of the finite-element model of an infinitely sloping soil column developed in this study is shown in Figure 4a, which illustrates the selection of elements and material models, boundary conditions for simulating groundwater and simple-shear deformation modes, and application of the earthquake ground motion at the base of the model. Further model details are provided in Makdisi (2016).

A test profile with a 2% slope inclination was evaluated. The test profile consisted of a 2-m-thick surficial crust, the bottom of which coincides with the groundwater table (GWT), underlain by a 3-m-thick continuous liquefiable layer with a relative density D_R of 50%. The liquefiable zone is underlain by a continuous layer of dense sand extending to a depth of 15 m; the deepest element in the model has a shear-wave velocity (V_s) of 600 m/s, which smoothly decreases in shallower elements at an impedance ratio of 1.03; the V_s in the liquefiable layer ranges from 120 to 140 m/s, and the shallowest element has a V_s of 75 m/s. All three layers were modelled using the constitutive model PM4Sand (Boulanger & Ziotopoulou, 2013), which is an effective stress, critical state-based, bounding-surface plasticity model capable of representing the generation of excess pore pressures, phase-transformation behaviour, and accumulation of progressive shear strains that have been observed in the dynamic response of loose, cohesionless soils. The PM4Sand model was calibrated in the liquefiable layer to replicate cyclic resistance to liquefaction observed in field data (e.g., Boulanger & Idriss, 2016); in the non-liquefiable layers, excess pore pressure generation was inhibited via a fixed, zero pore pressure boundary condition above the GWT (for the surficial crust layer), and via a PM4Sand calibration with a high contraction rate parameter to ensure a dilative response (for both the surficial crust and deeper dense sand layer). The static shear stress conditions representing the 2% slope inclination were simulated by adding a horizontal component to the element body forces in OpenSees.

Results from an example analysis of the soil profile are shown in Figure 4b for a historical record from the 1994 Northridge event (Record Sequence Number [RSN] 1004, LA – Sepulveda V.A. Hospital). This record is classified as being pulse-like, with a relatively short pulse period T_p of 0.93 seconds. The displacement time series at the top of Figure 4b indicates an initial displacement pulse of nearly 30 cm in the upslope direction that corresponds with the onset of liquefaction (based on the colormap of excess pore pressure time series in the middle plot of Figure 4b), which indicates immediate liquefaction (taken here as the pore pressure ratio r_u exceeding 0.90) throughout the liquefiable layer at a time of about 4 seconds. It is clear from the input velocity time series that the triggering of liquefaction coincides with the onset of the velocity pulse, and that subsequent deformations accumulate in the downslope direction while the soil is in its liquefied state.

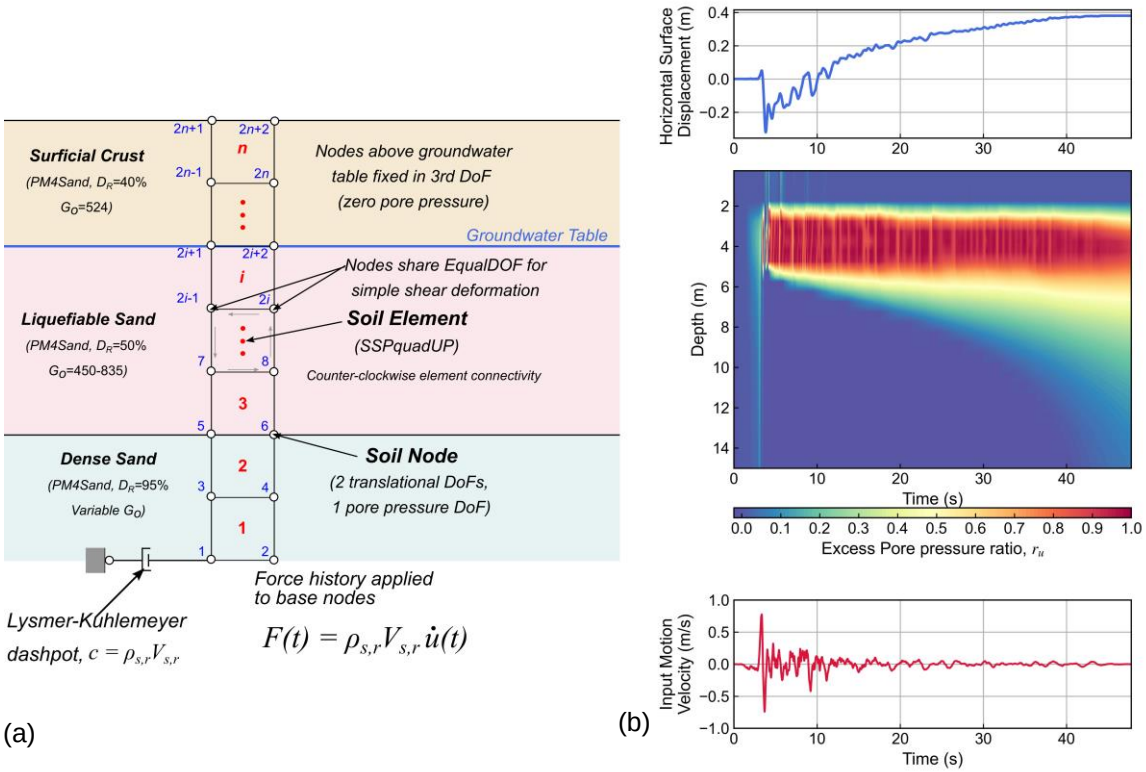

Figure 4: (a) Schematic of OpenSees model of infinitely sloping liquefiable soil column, and (b) example results from a single ground motion analysis, using RSN 1004 (L.A. Sepulveda V.A. Hospital) from the 1994 Northridge Earthquake.

3.2. Computational infrastructure

The 1,000 finite-element analyses in this study were performed using the Python library OpenSeesPy (Zhu et al., 2018) in an OpenSees cloud infrastructure, leveraging Amazon Web Services Cloud (AWS). The OpenSees AWS architecture primarily utilizes serverless services, designed for seamless, automated, and scalable resource management. A computational workflow was developed in OpenSeesPy for efficiently generating model realizations with varying ground motion inputs. These model realizations were executed in parallel using Elastic Cloud Compute (EC2) instances launched with an OpenSees Amazon Machine Image (AMI). Initialization of the OpenSees models, execution of the non-linear dynamic analyses, and post-processing of node and element recorder data were handled entirely on AWS, with output data stored in a private Simple Storage Service (S3) bucket.

4. Influence of near-fault ground motions on liquefaction response

The effects of near-fault ground motion characteristics on liquefaction were evaluated herein using the evolutionary IMs, PGA_M and *CAV*, in conjunction with a criterion for defining the time of liquefaction, t_L. This criterion was taken to be the time at which the first element in the OpenSees model exceeded an excess pore pressure ratio r_u of 0.90. Although multiple criteria could be used for assessing the time of liquefaction, such as alternative threshold r_u levels, peak cyclic shear strain thresholds, or Stockwell spectrogram-based methods (e.g., Greenfield, 2017), the r_u = 0.90 threshold correlated most closely with the onset of permanent deformations in the analyses performed in this study. The timing of liquefaction in a given analysis was then used to divide the PGA_M and *CAV* time series of the input motion into pre- and post-triggering ground-shaking portions to facilitate more precise analysis of IM-liquefaction demand relationships for both liquefaction triggering and permanent displacements.

4.1. Triggering of liquefaction and the liquefaction capacity intensity measure

The sensitivity of liquefaction triggering to ground motion intensity was evaluated using the concept of a "liquefaction capacity" IM, taken as the value of the input motion PGA_M or *CAV* at the time of liquefaction as

determined above. The liquefaction capacity IMs evaluated herein, denoted as $PGA_{M,L}$ and CAV_L, provide a convenient method for characterizing the liquefaction fragility (defined as the relationship between the IM level and the probability of liquefaction triggering) because the ground-shaking intensity at the time of liquefaction can be determined directly from the results of the numerical analyses using the criteria outlined at the beginning of this section. Lognormal distributions were fitted for the liquefaction-capacity IM values from the roughly 80% of cases (out of 1,000) in which liquefaction was observed for the example soil profile. Comparisons between the fitted distributions obtained from the full suite of ground motions, pulse-like, and non-pulse-like, are shown for $PGA_{M,L}$ and CAV_L in Figure 5a and Figure 5b, respectively. The data in Figure 5a indicate that the distribution of $PGA_{M,L}$ is largely insensitive to the pulse-like properties of near-fault ground motions, with a consistent median $PGA_{M,L}$ value of about 0.20 g and lognormal standard deviation of about 0.45 across both the pulse-like and non-pulse-like motions. Similarly, the pulse-like and non-pulse-like CAV_L distributions in Figure 5b are consistent with one another, with median CAV_L of around 1.80 m/s and lognormal standard deviations of around 0.40 to 0.45.

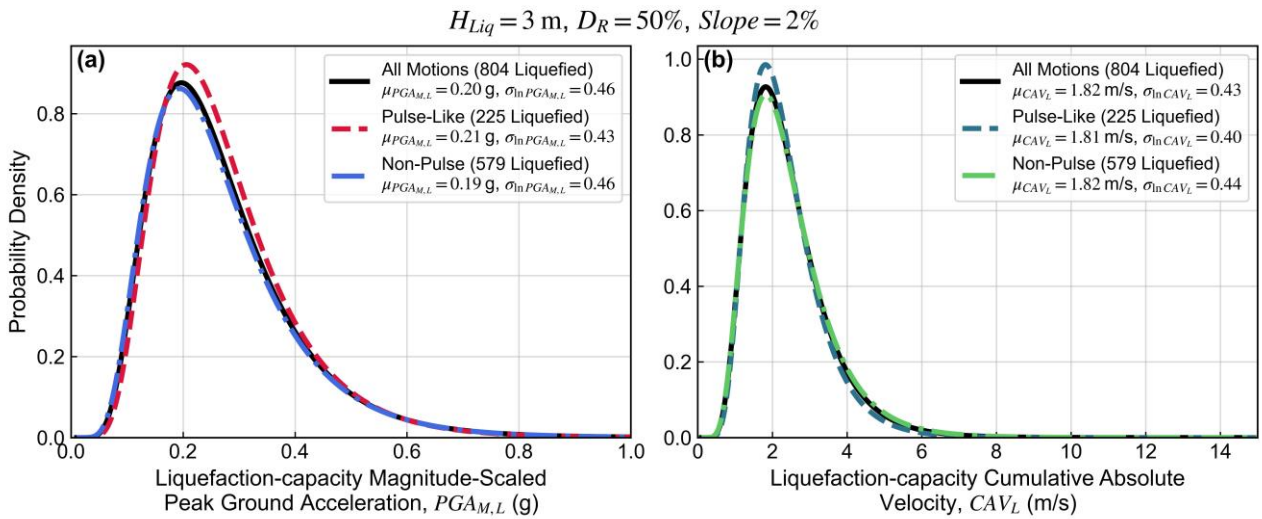

Figure 5: Fitted lognormal distributions of liquefaction capacity IMs for (a) PGA_M *and (b)* CAV *computed from simulated, near-fault motions representing the 1994 Northridge earthquake, used as inputs to a liquefiable OpenSees soil column model. Distributions are fit using only liquefied cases.*

4.2. Post-liquefaction response and permanent deformations

The sensitivity of permanent horizontal deformations to ground motion intensity was evaluated using the post-triggering proportion of a given evolutionary IM (i.e., PGA_M or *CAV*). The post-triggering IM values (IM_P) of PGA_M and *CAV*, denoted here as $PGA_{M,P}$ and CAV_P, were computed by subtracting the respective IM values at the time of liquefaction (defined in Section 4.1) from the total IM values of the full input ground motion time series. Simple linear models were fit to the natural logs of both the permanent displacements (*D*) and the post-triggering $PGA_{M,P}$ and CAV_P using ordinary least-squares regression from the 804 ground motions that caused liquefaction, the subset of pulse-like motions, and the subset of non-pulse-like motions. The fitted log-log models for each ground motion set are shown for $PGA_{M,P}$ in Figure 6a and for CAV_P in Figure 6b. The fitted ln(*D*)-ln(IM_P) relationships for the example soil profile analysis in Figure 6 appear to be reasonably consistent between pulse-like and non-pulse-like motions, indicating that the post-triggering $PGA_{M,P}$ and CAV_P may be capable of capturing the effects of velocity pulses on post-liquefaction response without requiring additional information about the pulse occurrence and its characteristics. Note that CAV_P appears to be a more efficient predictor of displacements than $PGA_{M,P}$ (as evidenced by the lower conditional standard deviations of the displacement $\sigma_{\ln D|\ln IM_P}$ shown in the legends in Figure 6), as well as that both post-triggering IMs may *slightly* under-predict displacements in pulse-like motions at deformations below 15–20 cm if the predictions are based on non-pulse or all motions.

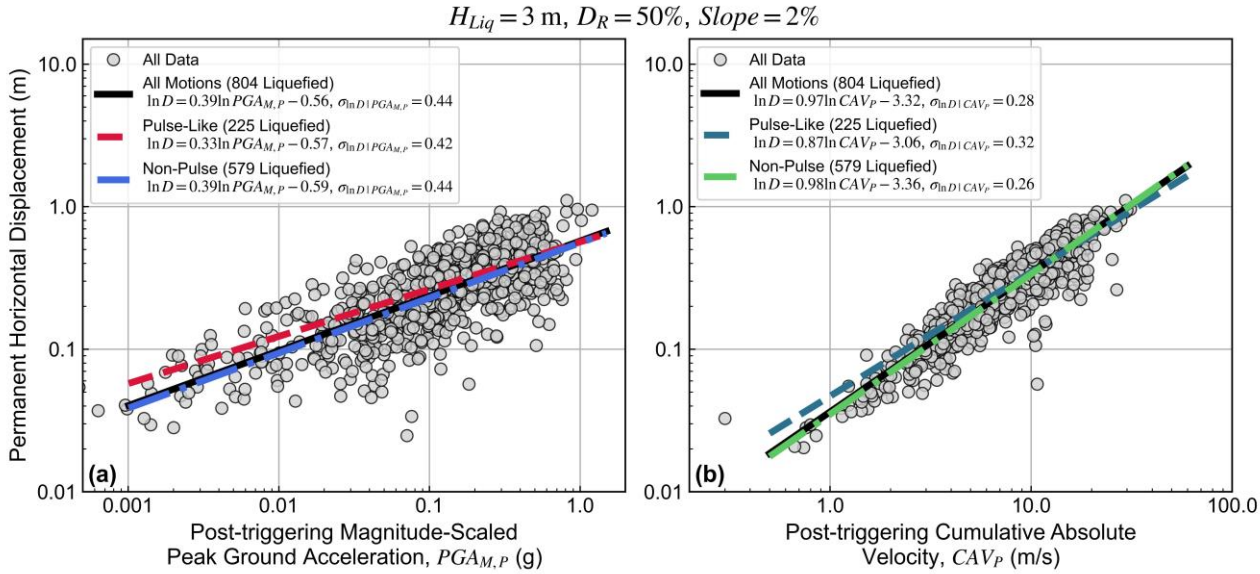

Figure 6: Fitted lognormal relationships between post-triggering intensity measures and permanent horizontal displacements, using (a) $PGA_{M,P}$ *and (b)* CAV_P *computed from simulated, near-fault motions representing the 1994 Northridge earthquake, used as inputs to a liquefiable OpenSees soil column model. Regression models are fit using only liquefied cases.*

4.3. Liquefaction response to simulated ground motion time series and historical records

An important aspect of using simulated ground motions in engineering applications (such as the evaluation of structural, geotechnical, or coupled system response) is demonstrating that engineering responses to simulated ground motions compare reasonably to those for historical records for scenarios where such data are available. Within the context of this study, the liquefaction responses (both liquefaction capacity and post-triggering deformations) of the example soil profile to the simulated 1994 Northridge ground motions are compared to their corresponding values from application of available historical records. An initial comparison of the responses can be made by performing the same non-linear analyses in OpenSees on the example soil profile (refer to Section 3.1) using the 36 historical records as inputs, and repeating the analysis of the output data in Section 4.1 (i.e., characterizing the liquefaction-capacity IM) and Section 4.2 (i.e., developing a simple regression model to describe the dependence of permanent displacement on the post-triggering IM).

Figure 7a shows the comparison of the distributions of liquefaction-capacity $PGA_{M,L}$ obtained from the 804 liquefaction-triggered cases using the 1,000 simulated ground motions, and the 27 (out of 36) liquefaction-triggered cases from the historical near-fault records. Despite the large differences in sample sizes, the PGA_L distributions for this example case are relatively consistent upon visual inspection, with the historical records producing a slightly lower capacity $PGA_{M,L}$ on average with moderately higher variability. Similar comparisons are made for the permanent displacement model in Figure 7b, using *CAV* as the post-triggering IM (CAV_P). The scattered CAV_P-*D* datapoints in Figure 7 indicate reasonable agreement between the OpenSees model results using the simulated and historical data, and the fitted regression lines and reported model errors are relatively consistent with one another.

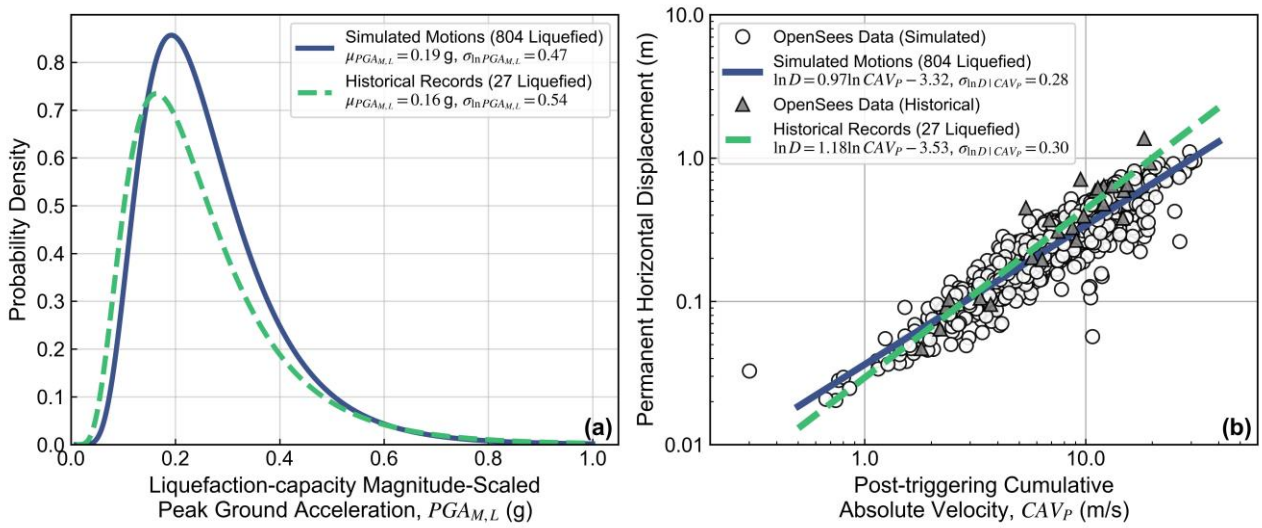

Figure 7: Comparison of (a) fitted distributions of liquefaction capacity $PGA_{M,L}$ and (b) regression models for post-trigging CAV_P and permanent displacements, developed using both simulated near-fault ground motions representing the 1994 Northridge earthquake and historical near-fault records from the same event.

5. Discussion and concluding remarks

The influence of near-fault ground motions on liquefaction triggering and lateral spreading were investigated using non-linear models of a hypothetical liquefiable soil column in OpenSees, subjected to ground motion simulations that linear models of a hypothetical liquefiable soil column in OpenSees, subjected to near-fault ground motion simulations that generated pulse-like and non-pulse-like records. The simulated ground motion sets were based on a parametric stochastic model and were developed for a range of source and path parameters to represent a realistic variability of ground motion intensities (IMs).

The analysis and results presented in this study, while relatively limited in scope, indicate that the potential effects of near-fault ground motion characteristics on liquefaction response are reasonably captured when evolutionary intensity measures (such as PGA_M and *CAV*) are considered. Furthermore, the results demonstrate the advantages of using a framework that accounts for the timing of liquefaction. It is likely that, in most of the cases evaluated in this study, the velocity pulse is what triggered the onset of liquefaction; therefore, a prediction framework centered around estimating the *capacity* IM of a liquefiable soil layer, in which the ground-shaking intensity required to trigger liquefaction depends on the soil's resistance to liquefaction (e.g., relative density, fines content, initial static shear stress), may be more likely to capture the effects of near-fault velocity pulses on the liquefaction response. This capacity-type framework can be contrasted with a more traditional fragility approach, in which a probability of liquefaction is developed from the total IM of the time series based on the observed proportion of liquefaction and non-liquefaction cases (the latter is often referred to as a "bounding-failure excitation" approach, e.g., Porter et al., 2007).

5.1. Implications for liquefaction-related research

The analyses of the example soil profile also provide some further indication that PGA_M and *CAV* are appropriate evolutionary IMs to use in the evaluation of liquefaction triggering and lateral spreading displacements, supporting previous studies from Kramer & Mitchell (2006), Kramer et al. (2016), Dashti & Karimi (2017), and Bullock et al. (2022). Although further analysis on a broader range of conditions could help to validate the conclusions drawn from this study, the data in Figures 5 and 6 appear to validate the use of PGA_M and CAV in near-fault conditions, an aspect of the liquefaction triggering problem that was not considered in the studies referenced above.

Furthermore, the stochastically simulated ground motions generated in this study, along with their propagation through a numerical model representing a liquefiable soil column, present a useful proof of concept for how simulations (of both strong ground motions and their subsequent impacts on geotechnical systems) can be used to fill critical knowledge gaps in earthquake engineering. As summarized in Table 2, 36 near-fault records exist from the 1994 Northridge earthquake; per the Next-Generation Liquefaction database (Brandenberg et

al., 2020), liquefaction was observed and documented at five sites within 15 km of the epicenter in the same earthquake, with none of the observations occurring at strong-motion stations. Drawing important, systematic conclusions that can be used in estimation of future liquefaction events would be exceedingly difficult from this amount of field data, motivating the need for simulation methods that are (1) calibrated to what has been observed in the field and laboratory, (2) used to assess the sensitivity of liquefaction-related hazards to a much wider and higher-resolution range of ground motion and site conditions, and (3) validated against historical observations where they exist.

5.2. Implications for validation of ground motion simulations

The concepts and results presented in Section 4.3 also provide another method for validating simulated ground motions, by considering the broad motivations for ground motion simulation (i.e., assessing engineering impacts) and how they are often used by researchers and practicing engineers (i.e., as inputs to structural or geotechnical models). Although it is important to ensure that the resulting ground motion amplitude, frequency content, and duration of the simulated ground motions matches what has been observed in historical data (Figure 2 and Figure 3), it is even more critical to have confidence that ground motion simulations produce reasonable engineering demand parameters (e.g., peak shear forces or drifts in structures, excess pore pressure generation or liquefaction-induced deformations in geotechnical systems) when used in numerical models. Although comparison of responses in a single structural or geotechnical model (such as the example soil profile considered herein) to simulated motions and historical records presents a good starting point for simulation validation, more robust validation across a broad range of models and conditions may require a more systematic, generalized characterization of engineering responses such as the IM-liquefaction demand relationships developed in this study. The dataset used to develop the capacity $PGA_{M,L}$ and CAV_L relationships in Figure 5 and the displacement regression models in Figure 6 for the example profile can be extended to include systematic dependence on soil and site conditions using a broader set of soil profiles. From a validation standpoint, the inclusion of more explanatory variables in these fragility and vulnerability representations would make the type of visual inspection in Section 4.3 less feasible, thereby motivating more rigorous and consistent quantification of the similarity between the liquefaction responses as derived from historical and simulated data (potentially using more objective statistical tests, such a *t*-tests or analysis of covariance).

5.3. Limitations and future work

The parameter space of the stochastically simulated ground motions and geotechnical conditions explored in this study are relatively limited. Although a large number of time series were generated, resulting in a wide range of IMs and substantial proportions of pulse-like motions, these 1,000 time series were from a single earthquake scenario occurring on a single type of rupture mechanism, and propagated through a single soil profile with idealized subsurface conditions. Therefore, the conclusions drawn from this study and their implications discussed above warrant being treated with caution. Future efforts to extend this work would include developing simulated near-fault motions from a broader range of source types and magnitudes; from a validation standpoint this may include expanding the suite of historical earthquakes to include those with a sufficient number of pulse-like motions (e.g., 1989 Loma Prieta, California; 1999 Chi-Chi, Taiwan; 2011 Christchurch, New Zealand). In conjunction with a broader set of soil profiles (e.g., variable liquefiable layer thicknesses, relative densities, and depths, as well as sloping ground conditions), this expanded dataset would allow for (1) more rigorous assessment of near-fault effects on liquefaction triggering and consequences, (2) evaluation of strategies for liquefaction fragility and vulnerability development that best capture these effects (e.g., a timing-based framework, identifying optimal intensity measures), and (3) development of robust and repeatable GMSV methods and criteria within the context of liquefaction.

6. Acknowledgments

The authors would like to acknowledge and thank Sean Ahdi, Kyle Withers, Nicolas Luco, Brian Shiro, and Janet Carter for their thoughtful comments and feedback, which greatly improved this paper. Any use of trade, firm, or product names is for descriptive purposes only and does not imply endorsement by the U.S. Government.

7. References

Baker, J. W. (2007). Quantitative Classification of Near-Fault Ground Motions Using Wavelet Analysis. *Bulletin of the Seismological Society of America*, *97*(5), 1486–1501. https://doi.org/10.1785/0120060255

Boore, D. M., Watson-Lamprey, J., & Abrahamson, N. A. (2006). Orientation-Independent Measures of Ground Motion. *Bulletin of the Seismological Society of America*, *96*(4A), 1502–1511. https://doi.org/0.1785/0120050209

Boulanger, R. W., & Idriss, I. M. (2016). CPT-Based Liquefaction Triggering Procedure. *Journal of Geotechnical and Geoenvironmental Engineering*, *142*(2), 04015065. https://doi.org/10.1061/(ASCE)GT.1943-5606.0001388

Boulanger, R. W., & Ziotopoulou, K. (2013). Formulation of a sand plasticity plane-strain model for earthquake engineering applications. *Soil Dynamics and Earthquake Engineering*, *53*, 254–267. https://doi.org/10.1016/j.soildyn.2013.07.006

Bozorgnia, Y., Abrahamson, N. A., Atik, L. A., Ancheta, T. D., Atkinson, G. M., Baker, J. W., Baltay, A., Boore, D. M., Campbell, K. W., Chiou, B. S.-J., Darragh, R., Day, S., Donahue, J., Graves, R. W., Gregor, N., Hanks, T., Idriss, I. M., Kamai, R., Kishida, T., … Youngs, R. (2014). NGA-West2 Research Project. *Earthquake Spectra*, *30*(3), 973–987. https://doi.org/10.1193/072113EQS209M

Brandenberg, S. J., Zimmaro, P., Stewart, J. P., Kwak, D. Y., Franke, K. W., Moss, R. E., Çetin, K. Ö., Can, G., Ilgac, M., Stamatakos, J., Weaver, T., & Kramer, S. L. (2020). Next-generation liquefaction database. *Earthquake Spectra*, *36*(2), 939–959. https://doi.org/10.1177/8755293020902477

Bullock, Z., Dashti, S., Liel, A. B., Porter, K. A., & Maurer, B. W. (2022). Probabilistic Liquefaction Triggering and Manifestation Models Based on Cumulative Absolute Velocity. *Journal of Geotechnical and Geoenvironmental Engineering*, *148*(3), 04021196. https://doi.org/10.1061/(ASCE)GT.1943-5606.0002729

Dabaghi, M., & Der Kiureghian, A. (2018). Simulation of orthogonal horizontal components of near-fault ground motion for specified earthquake source and site characteristics. *Earthquake Engineering & Structural Dynamics*, *47*(6), 1369–1393. https://doi.org/10.1002/eqe.3021

Dashti, S., & Karimi, Z. (2017). Ground Motion Intensity Measures to Evaluate I: The Liquefaction Hazard in the Vicinity of Shallow-Founded Structures. *Earthquake Spectra*, *33*(1), 241–276. https://doi.org/10.1193/103015eqs162m

Greenfield, M. W. (2017). *Effects of Long-Duration Ground Motions on Liquefaction Hazards* [University of Washington]. https://digital.lib.washington.edu/researchworks/handle/1773/40531?show=full

Kenawy, M., McCallen, D., & Pitarka, A. (2021). Variability of near-fault seismic risk to reinforced concrete buildings based on high-resolution physics-based ground motion simulations. *Earthquake Engineering & Structural Dynamics*, *50*(6), 1716–1733.

Kramer, S. L., & Mitchell, R. A. (2006). Ground Motion Intensity Measures for Liquefaction Hazard Evaluation. *Earthquake Spectra*, *22*(2), 413–438. https://doi.org/10.1193/1.2194970

Kramer, S. L., Sideras, S. S., & Greenfield, M. W. (2016). The timing of liquefaction and its utility in liquefaction hazard evaluation. *Soil Dynamics and Earthquake Engineering*, *91*, 133–146. https://doi.org/10.1016/j.soildyn.2016.07.025

Makdisi, A. J. (2016). *Liquefaction-Targeted Ground Motion Parameters* [University of Washington]. https://digital.lib.washington.edu/researchworks/handle/1773/47028

McKenna, F., Scott, M. H., & Fenves, G. L. (2010). Nonlinear Finite-Element Analysis Software Architecture Using Object Composition. *Journal of Computing in Civil Engineering*, *24*(1), 95–107. https://doi.org/10.1061/(ASCE)CP.1943-5487.0000002

Porter, K., Kennedy, R., & Bachman, R. (2007). Creating Fragility Functions for Performance-Based Earthquake Engineering. *Earthquake Spectra*, *23*(2), 471–489. https://doi.org/10.1193/1.2720892

Rezaeian, S., & Der Kiureghian, A. (2008). A stochastic ground motion model with separable temporal and spectral nonstationarities. *Earthquake Engineering & Structural Dynamics*, *37*(13), 1565–1584. https://doi.org/10.1002/eqe.831

Rezaeian, S., Petersen, M. D., & Moschetti, M. P. (2015). Ground Motion Models Used in the 2014 U.S. National Seismic Hazard Maps. *Earthquake Spectra*, *31*(1_suppl), S59–S84. https://doi.org/10.1193/111714EQS194M

Zhu, M., McKenna, F., & Scott, M. H. (2018). OpenSeesPy: Python library for the OpenSees finite element framework. *SoftwareX*, *7*, 6–11. https://doi.org/10.1016/j.softx.2017.10.009